Module 5C - 3D-Printed Food: Pumping a Food Slurry Through a Tube

Omar Betancourt, Payton Goodrich, Emre Mengi

July 24, 2021

Contents

Objectives: To learn how to model a common food processing technique - pumping a viscous food slurry through a tube.
Prerequisite Knowledge: High school physics, Fluid Dynamics, Basic Mechanics
Prerequisite Modules: 1A - Calculus, 1B - Linear Algebra, 1D - Differential Equations, 2A - Heat Transfer, 2B - Continuum Mechanics, 3C - Generic Time Stepping, 4A - Genetic Algorithms, 4B - Gradient-Based Optimization, 4C - Estimation and optimization of the effective properties of food mixtures
Difficulty: Hard
Summary: In this module, you will learn how to model a 'food pump' and use that model to find the pressure needed to force a viscous heterogeneous material through a small tube.
Objectives: Understanding irradiation, simulating the decontamination in industrial workplaces

Summary: In this module, you will learn about the physics involved in modeling viscous flow through a channel (tube). You will then complete a project that walks you through the modeling of a pumping system.

1 Theory

1.1 Introduction

Across many industries, new types of particle-laden materials are being developed and utilized. In the development of such materials, the basic philosophy is to select material combinations to produce desired aggregate responses upon deposition onto a substrate or into a mold. Oftentimes, such materials start in a fluidized form comprised of particles in a solvent or fluidized binder, forming a viscous slurry. However, because of the increasing demands for faster throughput and industrial-scale production of complex particle-laden materials, the determination of accurate pumping pressures is needed to move such fluids through delivery piping systems is critical (Figure **??**). There are a variety of related high-throughput industrial techniques, and we refer the reader to the surveys found in 17,18, as well as the works of 2, 23, 3, 4,5,6, 7,8 and 20,21). However, corresponding analysis in the food is somewhat lacking.
There have been monumental leaps in technologies associated with manufacturing technologies across many industries. These technologies have the potential to drastically improve food processing efficiency, food quality and safety. In particular the energy-efficient food production has become central many economies. Some approaches are methodical and systematic, while some are ad-hoc and haphazard. The purpose of this paper is to explore modeling and simulation themes associated with multiphase fluid flow and thermal food processing.
Many food and beverage manufacturers control their continuous fluid processes with PID algorithms, using data from downstream sensors to adjust flow and heating parameters, for example in pasteurization or sterilization processes. As food and beverage manufacturing looks to optimize production efficiencies and energy productivity, machine learning and other data science tools offer a chance to improve precision and predictive capabilities for real-time process optimization. In particular, new foods, such as plant-based meats, such as Beyond Meat $https://www.beyondmeat.com/$ and Impossible Burger $https://impossiblefoods.com/$ present new opportunities and challenges. However, for such procedures to be successful, rapidly computable models are needed to drive these technologies. In particular, to print fine-scale features for speciality foods, such as collagen-laden fibrous foods is a challenge, but could draw upon the large number of methods developed for 3D printing and printed electronics (See Zohdi [26,27]).

1.2 Technological approach

The main objective of this module is to develop a relatively simple model for the pressure gradients needed to move fluids containing charged particles as a function of (1) the volume fraction of added particles, (2) the pipe radius, (3) the volumetric flow rate, (4) the fluid-induced intensity of the shear stress at the pipe wall and (5) the base fluid viscosity. Overlayed on this are the induced thermal fields and associated material thermal dependency of the materials parameters in the system. As mentioned previously, this has become increasingly more important to 3D printing industry, which is attempting to rapidly print complex electrical inks ("e-inks"), where the embedded particles endow the cured printed materials with overall (mechanical,

electrical, thermal, magnetic, etc.) properties that the pure solvent (particle-free ink) alone does not possess. *The intension for this paper is to adapt and further these analysis for food production methods.*
An overall objective of the analysis is to develop semi-analytical expressions that can help guide analysts who are designing manufacturing systems involving fluidized particle-laden foods. Theoretically speaking, one could attempt a large-scale CFD analysis, however, for accurate direct numerical simulation of particle-laden continua, the spatial discretization grids must be extremely fine, with several thousand numerical unknowns needed per particle length-scale. Furthermore, extremely fine time-discretization is required. Thus, for even a small system with several hundred-thousand particles, a proper discretization would require several billion numerical unknowns (see, for example, 16, 19, 1, 27 and 26). Although such simulations are possible in high-performance computing centers, their usefulness for rapid daily design analysis for foods and related materials is minimal. This is even more critical if the models are used to drive real-time control. *Therefore, in this module we seek to develop simplified approaches.* This module presents analytical calculations to predict the pressure required to pump a suspension of rigid particles in an idealized fluid through a pipe of circular cross-section, under the assumption that the flow is uni-directional and fully developed. It first arrives at an analytical modification of Poiseulle flow through a pipe. The analysis assumes the suspension can simply treated as a homogenous fluid with an effective viscosity μ^*. This is a simplification, in order to develop useful and practical analytical results, without having to resort to computationally-intensive numerical methods which seek to calculate μ^* from detailed accounting of the micro-scale hydrodynamic interactions between particles in a suspension. Heat is also applied as a function of an externally-applied electric field.

1.3 Fluid through a pipe of radius R

We consider a fluid that is capable of carrying an electrical charge. Taking an annular element and summing the pressure and shear forces in the axial direction, along with uniform electrical body force, yields

$$-\frac{\partial P}{\partial x}+\frac{1}{r}\frac{\partial(r\tau)}{\partial r}=0\Rightarrow\frac{1}{r}\frac{\partial(r\tau)}{\partial r}=\frac{\partial P}{\partial x}. \tag{1.1}$$

Integrating yields

$$\tau=\frac{r}{2}\left(\frac{\partial}{\partial x}\right)+\frac{C_1}{r}=\mu^*\frac{\partial v}{\partial r}. \tag{1.2}$$

Integrating again yields

$$v(r)=\frac{1}{\mu^*}\left(\frac{r^2}{4}\left(\frac{\partial P}{\partial x}\right)+C_1 lnr\right)+C_2. \tag{1.3}$$

$v(r=0)$ must be finite, thus $C_1=0$, and $v(r=R)=0$ yields

$$v(r)=-\frac{R^2}{4\mu^*}\left(\frac{\partial P}{\partial x}\right)\left(1-(\frac{r}{R})^2\right) \tag{1.4}$$

Note that $v(r)$ is a maximum where

$$\frac{\partial v}{\partial r}=0=\frac{R^2}{4\mu^*}\left(\frac{\partial P}{\partial x}\right)\frac{2r}{R^2}, \tag{1.5}$$

which is at $r=0$. Thus,

$$v_{max}=v(r=0)=-\frac{R^2}{4\mu^*}\left(\frac{\partial P}{\partial x}\right)\Rightarrow v(r)=v_{max}\left(1-(\frac{r}{R})^2\right) \tag{1.6}$$

If we assume that the flow rate is constant

$$Q=Q_o=\int_A v\,dA=\frac{\pi v_{max}R^2}{2}\Rightarrow v_{max}=\frac{2Q_o}{\pi R^2}, \tag{1.7}$$

and we obtain

$$v(r) = \frac{2Q_o}{\pi R^2}\left(1 - (\frac{r}{R})^2\right) \tag{1.8}$$

The stress at becomes

$$\tau(r) = \mu^* \frac{\partial v(r)}{\partial r} = -\frac{4\mu^* Q_o r}{\pi R^4}. \tag{1.9}$$

The stress at the wall becomes

$$\tau_w = -\tau(r = R) = \frac{2\mu^* v_{\max}}{R} = \frac{4\mu^* Q_o}{\pi R^3}. \tag{1.10}$$

We have the following observations: (a) Increasing μ^* or Q_o increases the stress at the wall (τ_w) and (b) Decreasing R increases the stress at the wall (τ_w). In the remaining analysis, we will assume steady flow, the particles are not elongated and that they are well distributed within the base fluid.

1.4 Pressure gradients

The previous expressions allow us to correlate the pressure applied to a volume of particle-laden to allow it to move as a constant flow rate. By performing a force balance, we have in the positive x-direction (assuming steady flow, no acceleration)

$$(-(P + \Delta P) + P)\pi R^2 - \tau_w 2\pi R \Delta x = 0, \tag{1.11}$$

where x is the coordinate along the length of the pipe and Δx is the differential length, leading to

$$-\Delta P = \mu^* \frac{4Q_o}{\pi^2 R^5} 2\pi R \Delta x = 0, \rightarrow -\frac{\Delta P}{\Delta x} = -\frac{\partial P}{\partial x} = \frac{8\mu^* Q_o}{\pi R^4}, \tag{1.12}$$

where we used the expression for v_{max} and where the effective viscosity is a function of the volume fraction of particles, $\mu^* = \mu^*(\nu_p)$. An explicit relation for $\mu^*(\nu_p)$ will be given shortly. Solving for the pressure gradient yields

$$-\frac{\Delta P}{\Delta x} = -\frac{\partial P}{\partial x} = \underbrace{\frac{8\mu^*}{\pi R^4}}_{C} Q_o C Q_o. \tag{1.13}$$

If we fix the flow rate Q_o, the multiplier C identifies the pressure gradient needed to achieve a flow rate Q_o. For small pipes this can be a problem, as indicated by the R^4 term in the denominator.

1.5 Induced thermal fields via Joule heating

Process heating in food and beverage production facilities is typically accomplished with steam-heated heat exchangers. Most commonly, low pressure steam heats a plate and frame or tubular heat exchanger. For thermally sensitive food products, typical industry practice is to heat food in long tubular heat exchangers using flowing hot water, heated via direct steam injection, maintained at a single static temperature. Both steam-heated (single loop) and hot water heated (double-loop) heating processes are notoriously slow to reach processing temperature or adapt temperature to changing processing conditions. In particular, industrial-scale double-loop systems can take up to 10 minutes to create a response in end-target heating. Steam-powered heat exchange, in either single loop or double loop systems, is optimized for production in large facilities where processing conditions remain static and unchanging. These systems are optimized for traditional manufacturing operations and do not have the capabilities needed for the future. As this manufacturing sector moves towards shorter production runs and expanding the number of products produced in a single production line, there is an opportunity to find new production efficiencies and increase energy productivity to boost yields and facility operational effective efficiency (OEE). Induction heating adapts well to computer control and allows for instantaneous control, currently limited by the sensitivity and response time of a downstream thermocouple. It is for this reason that we select induction hearting as a model process. From the first law of thermodynamics, we have the following description of Watts per unit volume:

$$\rho^* C^* \dot{\theta} = H - S \tag{1.14}$$

where H represents heating and S represents sinks. For the heating

$$H = a\frac{J^2}{\sigma^*}, \tag{1.15}$$

where a is the absorption coefficient, and S represents all of the losses (conductive, convective, radiative, refrigeration). Discretizing and solving yields

$$\theta(t+\Delta t) = \theta(t) + \frac{\Delta t}{\rho^* C^*}(H - S) = \theta(t) + \frac{\Delta t}{\rho^* C^*}(a\frac{J^2}{\sigma^*} - S(t)) \tag{1.16}$$

If at a given time t, we want $\theta(t+\Delta t) = \theta^*$ can solve for the necessary $J(t)$:

$$J(t) = \sqrt{\frac{\sigma^*}{a}\left(\rho^* C^* \frac{\theta^* - \theta(t)}{\Delta t} + S(t)\right)}. \tag{1.17}$$

1.6 Models for effective properties of particle-laden fluids

A key component of the analysis requires the characterization of the effective properties of a particle-laden fluid as a function of the volume fraction of particles and the baseline (interstitial) fluid properties. The density of the particle-laden fluid is actually an "effective density", since it actually is a mixture of materials (particles and interstitial fluid). Effective properties are defined through volume averages. For example, the effective density of the mixture is

$$\rho^* \langle \rho() \rangle_V \frac{1}{V}\int_V \rho()\, dV = \frac{1}{V}\left(\int_{V_f} \rho_f\, dV + \int_{V_p} \rho_p\, dV\right) = \nu_f \rho_f + \nu_p \rho_p \tag{1.18}$$

where ν_f and ν_p are the volume fractions of the fluid and particles, respectively. The volume fractions have to sum to unity: $\nu_f + \nu_p = 1 \Rightarrow \nu_f = 1 - \nu_p$. Similar approaches can be used to calculate various types of properties, such as the effective viscosity. However, to calculate it is somewhat more complicated, since it requires one to estimate the interaction between the constituents. There are a number of models which provide expressions for the effective viscosity of the fluid containing particles. One of the first models for the effective viscosity of such fluids was developed in 1906 by 9. It reads as

$$\mu^* = \mu_f(1 + 2.5\nu_p), \tag{1.19}$$

where μ^* is the effective viscosity, μ_f is the viscosity of the fluid and ν_p is the volume fraction of particles. This expression is accurate only for low volume fractions of particles. A more accurate approximation, *in fact a strict, rigorous, lower bound* (accurate up to approximately $\nu_p = 20\%$, which is sufficient for most applications of interest) can be derived from the well-known Hashin and Shtrikman bounds (11,12, and 13) bounds in solid mechanics. Specifically, for linearized elasticity applications, for isotropic materials with isotropic effective (mechanical) responses, the Hashin-Shtrikman bounds (for a two-phase material) are as follows for the effective bulk modulus (κ^*)

$$\kappa^{*,-}\kappa_1 + \frac{\nu_2}{\frac{1}{\kappa_2-\kappa_1} + \frac{3(1-\nu_2)}{3\kappa_1+4\mu_1}} \leq \kappa^* \leq \kappa_2 + \frac{1-\nu_2}{\frac{1}{\kappa_1-\kappa_2} + \frac{3\nu_2}{3\kappa_2+4\mu_2}}\kappa^{*,+} \tag{1.20}$$

and for the effective shear modulus (G^*)

$$G^{*,-}G_1 + \frac{\nu_2}{\frac{1}{G_2-G_1} + \frac{6(1-\nu_2)(\kappa_1+2G_1)}{5G_1(3\kappa_1+4G_1)}} \leq G^* \leq G_2 + \frac{(1-\nu_2)}{\frac{1}{G_1-G_2} + \frac{6\nu_2(\kappa_2+2G_2)}{5G_2(3\kappa_2+4G_2)}}G^{*,+}, \tag{1.21}$$

where κ_1 (usually the matrix material) and κ_2 (usually the particulate material) are the bulk moduli and G_1 and G_2 are the shear moduli of the respective phases ($\kappa_2 \geq \kappa_1$ and $G_2 \geq G_1$), and where ν_2 is the second phase volume fraction. Such bounds are the tightest possible on isotropic effective responses, with isotropic two phase microstructures, where only the volume fractions and phase contrasts of the constituents are known

(see13 for a discussion on the optimality of such bounds). Note that no geometric or statistical information is required for the bounds. For an authoritative review of the general theory of random heterogeneous media see 25. One can take the limit of the particle phase becoming rigid, i.e. the bulk and shear moduli tending towards infinity, $\kappa_2 = \kappa_p \to \infty$ and $G_2 = \mu_p \to \infty$, signifying that the particles are much stiffer than the interstitial fluid, while simultaneously specifying that the interstitial fluid is incompressible, i.e. $\kappa_1/G_1 = \kappa_f/\mu_f \to \infty$ with G_1 being finite. This yields,

$$\mu^* \geq \mu^{*,-} = \mu_f \left(1 + 2.5\frac{\nu_p}{1-\nu_p}\right). \tag{1.22}$$

Equation 1.22 represents the tightest known lower bound on the effective viscosity of a two-phase material comprised of rigid particles in a surrounding incompressible fluid. The bound recapture the Einstein result in the $\nu_p \to 0$ limit, but is a rigorous lower bound at significant ν_p. *This rigorous lower bound* is extremely accurate up to approximately 20 % volume fraction. These bounds have been tested in the numerical analysis literature repeatedly, for example against direct Finite Element calculations found in 26. We refer the reader to 15 for more in depth analysis on the effective viscosity of particle-laden fluids see 24 for the analysis of the proper application of the non-interaction and the "dilute limit" approximations and for detailed discussions on the isotropic and anisotropic viscosity of suspensions containing particles of diverse shapes and orientations. It is important to emphasize that 15 is accurate for up to 25-30 % in case of spherical particles. Furthermore, 15 covers other shapes, including, importantly, mixtures of diverse shapes. Of course, one can one employ formulas such as in 15 for more accuracy, however, because the Hashin-Strikman expression is a strict lower bound, $\mu^{*,-} \leq \mu^*$, we consequently generate a strict lower bound for the pressure gradient

$$-\frac{\partial P}{\partial x} \geq \underbrace{\frac{8\mu^{*,-}}{\pi R^4}}_{C^-} Q_o C^- Q_o. \tag{1.23}$$

1.7 Thermal behavior

The primary properties which change are the viscosity and electrical conductivity. For example, for the viscosity

$$\mu_f = \mu_{fo} e^{-k_1 \frac{\theta-\theta_o}{\theta_o}}, \tag{1.24}$$

and

$$\sigma_f = \sigma_{fo} e^{-k_2 \frac{\theta-\theta_o}{\theta_o}}, \tag{1.25}$$

and

$$\sigma_p = \sigma_{po} e^{-k_3 \frac{\theta-\theta_o}{\theta_o}}. \tag{1.26}$$

1.8 Overall outlook

Currently, a modest level of modern technologies has been implemented in food production. For example, sensors, cameras, telecommunications have not been widely deployed. Furthermore, the cost of specialized equipment has been prohibitive and development of coherent, easy-to-use, rapid data fusion/management systems across different platforms is lacking. Additionally, while control systems exist, they simply are too slow to be useful in deployed mobile computing platforms in harsh environments. The long term mission of this research is to integrate and implement convergent research in the development of smart, robust and inexpensive systems that are easy to maintain, upgrade and deploy, incorporating state-of-the-art technologies. A key to much of this work is the transfer of advances in the fields of Advanced Manufacturing and Computational Science to food production. In particular, digital-twin-enabled, simulation-sensor fusion, which refers to a digital replica of physical systems, is a key, Digital twins blend artificial intelligence, machine learning, and software analytics with data to create living digital computer models that can update and change in

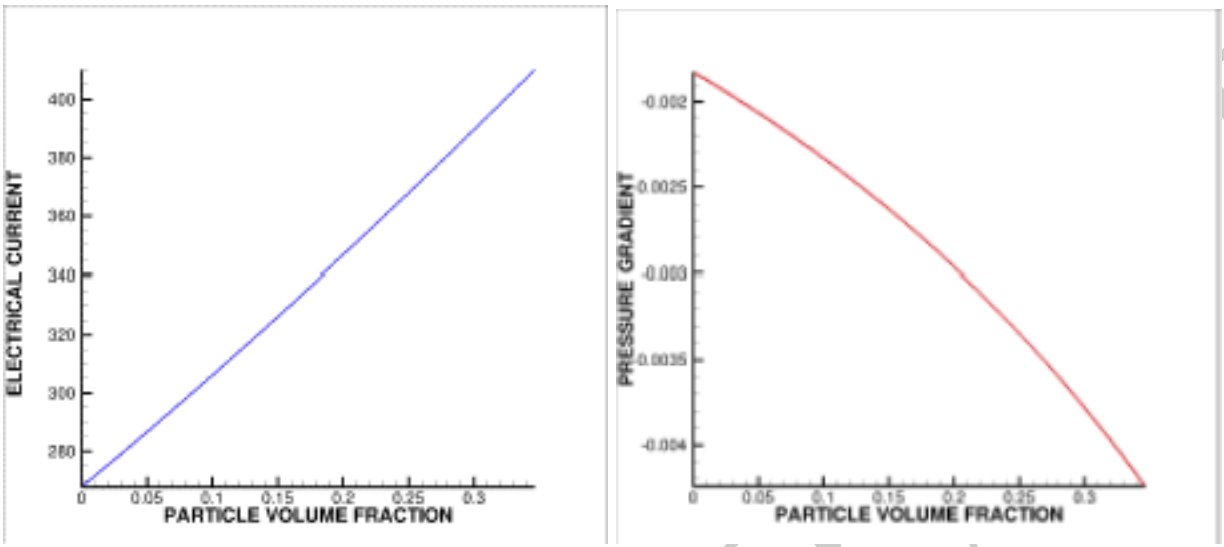

Figure 2.1: LEFT: The electric field needed for the volume fraction of particles. RIGHT: The pressure gradient needed ($\frac{\Delta P}{\Delta x}$) as a function of volume fractions of ν_p.

tandem with their physical counterparts. We will seek to enable real-time simulation of processing devices to operate in tandem with their deployed response. Updates to the digital twin are made continuously in near real-time, which necessitates rapid wireless communication, hyperspectral cameras and sensor fusion, and rapid simulation of process behavior. The digital twin concept should quickly ascertain a) fault behavior by utilizing the best available data. Today, there is no shortage of simulation codes; however, the fundamental limitations are real-time accuracy and deployable in-the-field use in harsh environments. A core issue across all domains of application is extreme flexibility—the ability of a system to adapt to rapid changes in the environment and system capabilities by autonomously modifying tasks and then apply various problem-solving approaches. In this context, a goal will be to make fundamental advances in several coupled autonomy-related fields to increase functional flexibility, while being constrained by the multiple aspects of variable system capabilities and operation in complex environments. These methods should be benchmarked and validated against an extensive suite of experimental tests. This has several potential impacts and benefits to member organization.

2 Example

For the theory discussed in the previous section, we plotted the pressure gradient as a function of of ν_p, with the following parameters:[1] (a) viscosity, $\mu_f = 0.01\,Pa - s$, (b) fluid density: $\rho_f = 1000\,kg/m^3$, (c) particle density: $\rho_p = 2000\,kg/m^3$, (d) flow rate: $Q_o = 0.00001\,m^3/s$, (e) thermal sensitivity: $k_1 = k_2 = k_3 = 1$, and (f) pipe radius: $R = 0.01\,m$. The goal is the raise the temperature from 300 K to 400 K in 1 second. The plots are shown in Figures 2.1-2.2. The pressure gradient steadily increases with particle volume fraction. Due to the increase in the particle volume fraction, the viscosity increases, thus decreasing the Reynolds number (already quite small). The point of this example was not to illustrate an all encompassing parameter set, but simply to show the explicit dependency of the pressure gradient on the presence of secondary particles.

[1]For reference, the viscosity of water is $\mu_f = 0.001\,Pa - s$ and for honey, $\mu_f = 1\,Pa - s$.

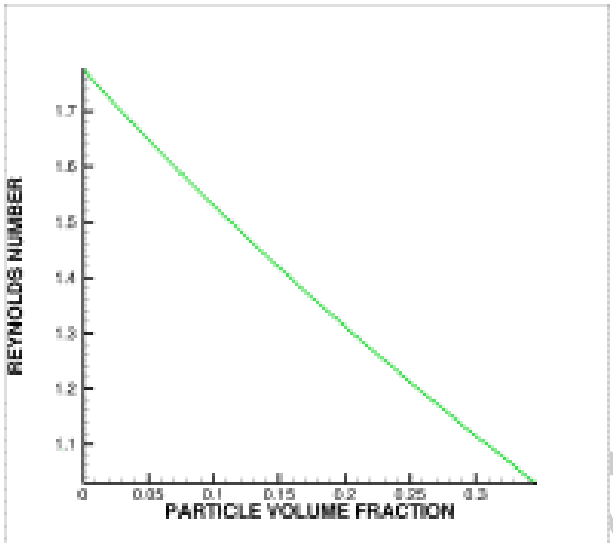

Figure 2.2: The resulting Reynolds number.

3 Assignment

In this assignment, we will model the extrusion of a two-phase food slurry consisting of small particles suspended in a binder. Such slurries can have very high viscosities, making them challenging to print through small nozzles if the process is not controlled carefully. In this project, you will use a quasi-1D flow model to assess the impact of different processing parameters on the pressure gradients and nozzle wear rates that the equipment will experience while printing with different process parameters.

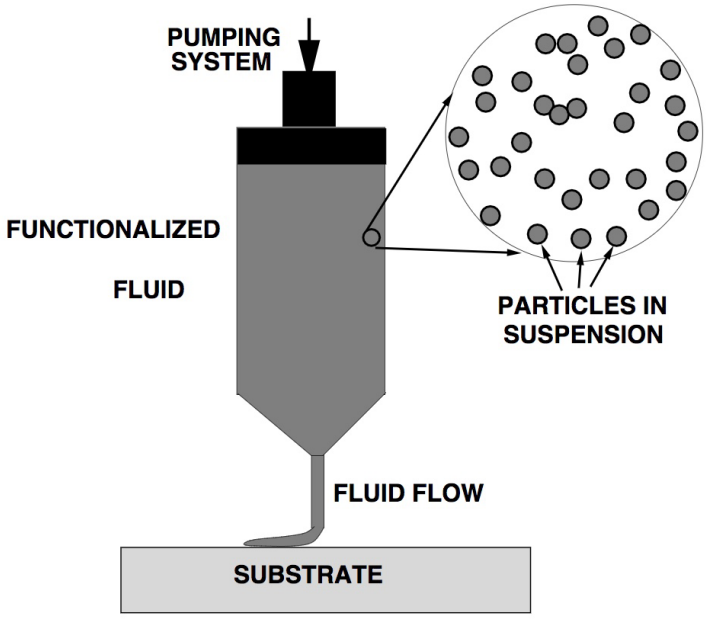

Figure 3.1: Schematic of printing

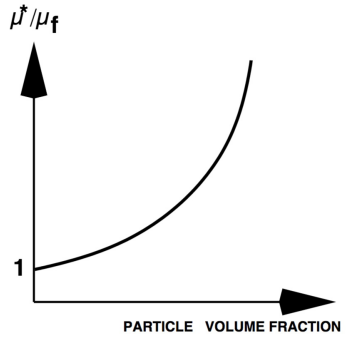

Figure 3.2: Relationship between particle volume fraction and effective viscosity.

EXTRUSION & PRESSURE GRADIENTS

Channel Flow:

The objective of the first part of this analysis is to derive a model for the pressure gradient required to maintain a given flow rate in a channel, as a function of the volume fraction of particles present in the slurry, and the temperature of the slurry. Consider an idealized channel with a circular cross-section of area $A = \pi R^2$, with a velocity profile of the form:

$$v(r) = v_{\max}\left(1 - \left(\frac{r}{R}\right)^q\right), \tag{3.1}$$

where $v_{\max}$ is the center line velocity and r is the radial coordinate from the center line of the channel. For fully developed laminar flow, $q = 2$. Higher q values correspond to increasingly turbulent flow. The shear stress in the fluid is given by

$$\tau(r) = \mu^* \frac{\partial v}{\partial r} = -\frac{\mu^* v_{\max} q}{R}\left(\frac{r}{R}\right)^{q-1}, \tag{3.2}$$

where μ^* is the effective viscosity of the slurry. The total flow rate is treated as a known constant:

$$Q = \int_A v\, dA = Q_o. \tag{3.3}$$

The centerline velocity can be rewritten in terms of the flow rate as follows:

$$v_{\max} = \frac{Q_o(q+2)}{Aq} = \frac{Q_o(q+2)}{\pi R^2 q}. \tag{3.4}$$

Plugging this expression for the velocity into the wall stress equation yields:

$$\tau_w = -\tau(r = R) = \frac{\mu^* v_{\max} q}{R} = \frac{\mu^* Q_o(q+2)}{\pi R^3}. \tag{3.5}$$

Pressure Gradients:

In the remaining analysis, we will assume that the fluid flow is steady, that the particles are not elongated and that they are mixed uniformly throughout the slurry.[1] The previous expressions allow us to correlate the flow rate of a particle-laden fluid to the shear stress the fluid exerts on the walls of a nozzle. From this shear stress, we can determine the pressure gradient required to maintain steady axial flow[2]:

$$(-(P + \Delta P) + P)\pi R^2 - \tau_w 2\pi R \Delta x = 0, \tag{3.6}$$

where Δx is a differential length along the axis of the pipe.

$$-\Delta P = \mu^* \frac{Q_o(q+2)}{\pi^2 R^5} 2\pi R \Delta x = \frac{2\mu^* Q_o(q+2)\Delta x}{\pi R^4}, \tag{3.7}$$

where we used the expression for v_{max} and where the effective viscosity is a function of the volume fraction of particles, $\mu^* = \mu^*(v_p)$. An explicit relation for $\mu^*(v_p)$ will be given shortly. Solving for the pressure gradient yields

$$-\frac{\Delta P}{\Delta x} = \underbrace{\frac{2\mu^*(q+2)}{\pi R^4}}_{C} Q_o C Q_o. \tag{3.8}$$

If we fix the flow rate Q_o, the multiplier C identifies the pressure gradient needed.

Velocity Profile Characteristics:

As the Reynolds number increases, the velocity profile will change from a quadratic ($q = 2$) to a more blunted profile ($q >> 2$). The effect of a changing profile is described by representing q as a function of the centerline Reynolds' number ($\mathcal{R}_{ec}$):

[1] Elongated particles tend to align themselves with the flow, which alters their impact on the viscosity.
[2] Steady flow means no acceleration.

$$q = q(\mathcal{R}_{ec}) = c_1\mathcal{R}_{ec} + c_2, \tag{3.9}$$

where $\mathcal{R}_{ec} = \frac{\rho^* v_{\max} 2R}{\mu^*}$ and c_1 and c_2 are constants. Usually, $0 \leq c_1 << 1$ and $c_2 \approx 2$. For the general case, combining Equation 3.4 with Equation 3.9 and the definition of the centerline Reynolds' number, we obtain a quadratic relationship for q,

$$q^2 - (\gamma^* + c_2)q - 2\gamma^* = 0 \tag{3.10}$$

where

$$\gamma^* = \frac{2c_1 Q\rho^*}{\pi R\mu^*}$$

ρ^* is the effective density, and μ^* is the effective viscosity. This quadratic relationship can be solved for q to yield:

$$q(\mathcal{R}_{ec}) = \frac{1}{2}\left((\gamma^* + c_2) \pm \sqrt{(\gamma^* + c_2)^2 + 8\gamma^*}\right) \tag{3.11}$$

JOULE HEATING

Joule heating is the process of pumping an electrical current through a mass to directly heat it. The process can be controlled precisely and could be adapted for use in future advanced food manufacturing. From the first law of thermodynamics, we have the following description of Watts per unit volume:

$$\rho^* C^* \dot{\theta} = H - S \tag{3.12}$$

where H represents heating power, S represents all of the losses (conduction, convection, radiation), ρ^* is the effective slurry density, C^* is the effective slurry heat capacity, and $\dot{\theta}$ is the time derivative of the temperature of the slurry, $\frac{d\theta}{dt}$. For the heating term, use Joule heating exclusively:

$$H = a\frac{J^2}{\sigma^*}, \tag{3.13}$$

where a is the absorption coefficient and J is the induced current within the slurry. Discretizing equation 3.12 and solving for the temperature yields:

$$\theta(t + \Delta t) = \theta(t) + \frac{\Delta t}{\rho^* C^*}(H - S) = \theta(t) + \frac{\Delta t}{\rho^* C^*}(a\frac{J^2}{\sigma^*} - S(t)) \tag{3.14}$$

If at a given time t, we want $\theta(t + \Delta t) = \theta^*$ can solve for the necessary $J(t)$:

$$J(t) = \sqrt{\frac{\sigma^*}{a}\left(\rho^* C^* \frac{\theta^* - \theta(t)}{\Delta t} + S(t)\right)} \tag{3.15}$$

The thermal loss term S can account for any kind of thermal loss. For this assignment, assume that the dominant mode of thermal loss to the environment is convection and that the temperature is essentially uniform within a cross-section of the pipe. Convective losses are often modeled by:

$$S = hA(\theta(t) - \theta_a))$$

Where h is the convection coefficient, A is the area over which conduction occurs, $\theta(t)$ is the temperature of the object being modeled at a given time, t, and θ_a is the temperature of the ambient environment. Since all of our other terms are per unit volume of the slurry, we must alter this relationship to have compatible units. Assume that we are considering an arbitrary length Δx of the pipe. The surface area A will be $2\pi R\Delta x$, and the total volume will be ${}^2\Delta x$. Dividing A by volume yields $1/R$. As such, the convective losses per unit volume will be:

$$S = h(\theta(t) - \theta_a)/R \tag{3.16}$$

Note that $S(t)$ models the transfer of heat *out of the system*, so a positive value of S represents a loss of energy.

EFFECTIVE PROPERTIES OF PARTICLE-LADEN FLUIDS

Thermal effects:

The temperature-dependent viscosity of the fluid mixture will change according to:

$$\mu_f(\theta) = \mu_{fo} e^{-k\frac{\theta(t)-\theta_o}{\theta_o}}, \tag{3.17}$$

$$\sigma_f(\theta) = \sigma_{fo} e^{-k_2\frac{\theta(t)-\theta_o}{\theta_o}}, \tag{3.18}$$

$$\sigma_p(\theta) = \sigma_{po} e^{-k_3\frac{\theta(t)-\theta_o}{\theta_o}}. \tag{3.19}$$

where μ_{fo} is the nominal viscosity of the fluid at $\theta = \theta_o$, σ_{fo} and σ_{po} represent the nominal electrical conductivity of the fluid and particles respectively at $\theta = \theta_o$, θ_o is the initial temperature of the slurry, and $[k_1,\ ,k_2,\ k_3]$ are experimentally determined thermal "softening" parameters. All other properties are assumed to change negligibly with temperature over the range of temperatures that will be encountered in this problem.

Effective Density:

It is important to characterize the effective properties of a particle-laden fluid as a function of the volume fraction of particles and the baseline (interstitial) fluid properties. The density of the particle-laden fluid is actually an "effective density", since it actually is a mixture of materials (particles and interstitial fluid). Effective properties are defined through volume averages. For example, the effective density of the mixture is:

$$\rho^* \langle \rho() \rangle_V \frac{1}{V} \int_V \rho()\, dV = \frac{1}{V}\left(\int_{V_f} \rho_f\, dV + \int_{V_p} \rho_p\, dV \right) = v_f \rho_f + v_p \rho_p \tag{3.20}$$

where v_f and v_p are the volume fractions of the fluid and particles, respectively. The volume fractions have to sum to unity, (i.e. $v_f + v_p = 1 \Rightarrow v_f = 1 - v_p$).

Effective Heat Capacity:

Similarly:

$$C^* \langle C() \rangle_V \frac{1}{V} \int_V C()\, dV = \frac{1}{V}\left(\int_{V_f} C_f\, dV + \int_{V_p} C_p\, dV \right) = v_f C_f + v_p C_p \tag{3.21}$$

where v_f and v_p are the volume fractions of the fluid and particles, respectively. The volume fractions have to sum to unity, (i.e. $v_f + v_p = 1 \Rightarrow v_f = 1 - v_p$).

Effective Viscosity:

Similar approaches can be used to calculate other physical properties of mixtures, such as the effective viscosity. However, to calculate them is a bit more complicated, since they require estimating mechanical interactions between constituents. There are a number of models which provide expressions for the effective viscosity of the fluid containing particles. For the purposes of this flow analysis, the particles are considered to be rigid relative to the surrounding fluid (e.g. almond bits in molten chocolate). There are several models for the effective properties of mixtures with different assumptions about the interaction of the constituent phases. As such, we would normally need to use the Hashin and Shtrikman bounds to obtain an lower and upper bound for the slurry viscosities ($\mu^{*,-}$ and $\mu^{*,+}$). However, we can take advantage of the large deviation of mechanical properties between the fluid and particles. One can take the limit of the particle phase becoming rigid, i.e. the bulk and shear moduli tending towards infinity, $\kappa_p \to \infty$ and $\mu_p \to \infty$, signifying that the particles are much stiffer than the interstitial fluid, while simultaneously specifying that the interstitial fluid is incompressible, i.e. $\kappa_f/\mu_f \to \infty$ with μ_f being finite. This yields:

$$\mu^* \geq \mu^{*,-} = \mu_f(1 + 2.5\frac{v_p}{1 - v_p}). \tag{3.22}$$

The expression in Equation 3.22 is the tightest known lower bound on the effective viscosity of a two-phase material comprised of rigid particles in a surrounding incompressible fluid. This expression remains quite accurate up to about $v_p = 0.25$, which is sufficient for most applications.

Effective Conductivity:

Unlike the effective viscosities shown above, the electrical conductivity is not as directly correlated to the properties of the fluid and particles in the slurry. As such, we can no longer simplify the Hashin-Shtrikman bounds as we did above for the viscosities, and must use the full bounds. The effective thermal conductivity estimates are, for two isotropic materials with an overall isotropic response:

$$\underbrace{\sigma_f + \frac{v_p}{\frac{1}{\sigma_p - \sigma_f} + \frac{1-v_p}{3\sigma_f}}}_{\sigma^{*,-}} \leq \sigma^* \leq \underbrace{\sigma_p + \frac{1-v_p}{\frac{1}{\sigma_f - \sigma_p} + \frac{v_p}{3\sigma_p}}}_{\sigma^{*,+}}, \tag{3.23}$$

Such bounds are the tightest known on isotropic effective responses, with isotropic two phase microstructures, where only the volume fractions and physical properties of the constituents are known. The typical use of these bounds is to form a convex combination of them as follows:

$$\sigma^* \approx \phi\sigma^{*,-} + (1-\phi)\sigma^{*,+}\sigma^{*,\phi} \tag{3.24}$$

- If $\phi = 0$ we have the lower bound,
- If $\phi = 1$ we have the upper bound,
- If $\phi = 1/2$ we have the average of the upper and lower bounds.

NOZZLE WEAR

The next property we want to model is the impact of wear on the nozzle over time. There will be a trade-off between the volume fraction of particles in the fluid, the print resolution and the expected lifetime of the nozzle. We consider a nozzle with radius R_o with a circular cross-sectional area of $A_0 = \pi R_o^2$. The objective is to describe the mechanism by which R changes, due to nozzle wall wear caused by fluid-induced shear stress. As a simplification, we assume that the wear is uniform around the circumference of the channel.

Interface wear:

We assume that wear of the nozzle wall is controlled by the intensity of the fluid-induced shear stress near the wall, where higher shear stresses increase the wear at the wall. We model the wear rate as being proportional to the normalized difference between the shear stress at the wall and the critical "wear" stress ($\tau^{crit} > 0$):

$$\frac{dR}{dt} = \eta * \max\left(\frac{\tau_w - \tau^{crit}}{\tau^{crit}}, 0\right) = \eta * \max\left(\frac{\mu^* Q_o(q+2)}{\pi\tau^{crit}R^3} - 1,\ 0\right) \tag{3.25}$$

where η is a rate constant representing the wear per unit time. If we assume fully developed laminar flow, then we can assume q. The steady state value of the channel radius, denoted R^{ss}, can then be determined analytically.

Note that, if q is not assumed constant, it will be a function of the radius by equation 3.11. This makes it very challenging to write a closed-form solution for R^{ss}. You can use a nonlinear solver such as Matlab's `fsolve()`, and include q as a function of R to solve the problem for non-constant q. This will **not** be required for this project, but this is a good extension if you would like to enhance the functionality of your simulation in the future.

Numerical Simulation:

In order to study the time-evolution of the wear, equation 3.25 is solved using forward Euler time integration:

$$R(t + \Delta t) = R(t) + \Delta t\mathcal{F}(R(t)). \tag{3.26}$$

PROJECT INSTRUCTIONS AND DELIVERABLES

Please address the following specific questions and incorporate them into a brief technical report that would be sufficient for another student not enrolled in this class to understand the theory and interpret your results.

PART 1: PUMPING PRESSURE & REYNOLDS NUMBER

For the first part of this assignment, you will determine the pressure gradient required to maintain a sinusoidally-varying flow rate while the temperature of the material also varies. You may assume the following:

- The flow is quasi-static (acceleration may be neglected).
- The fluid is heated uniformly (imagine that the flow is moving through an infinitely long pipe and that the heating current is uniform everywhere and started simultaneously).
- Heat sources other than the Joule heating (i.e. friction) are negligible.

The flow rate varies with time according to:

$$Q = Q_o(1 + bsin(\omega t)) \tag{3.27}$$

Assume that we want the mixture to heat up at a constant rate of 50 K/s.

1. Explain the impact of the simplifying assumptions made in modeling this problem. What is left out?
2. When presenting the formula for τ_w, explain which terms influence it and how.
3. Rederive and explain the pressure gradient expression. A figure or illustration may help.
4. Explain equation 3.11. Are both roots physically valid? If not, which one is correct and why? (*Hint: you should be able to answer this question by inspecting the equation and looking at how q is used. Something will go very wrong if you pick the incorrect root.*)
5. Use the fixed temperature increase rate and and assume that the mixture loses heat to the environment by convection only. Show how to use equations 3.15 and 3.16 to solve for $J(t)$.
6. Plot the current of the mixture as a function of time. Use a time step of $\Delta t_1 = .01s$, and a final time of $T = 2.5s$.
7. Plot the pressure gradient to maintain the time-dependent flow for $v_2 \in \{0, 0.05, 0.10, 0.15, 0.20, 0.25\}$. This should be *one figure* with 6 curves. Use a time step of $\Delta t_1 = .01s$, and a final time of $T = 2.5s$. Remember that the material properties are a function of temperature!
8. Plot the Reynolds number of the time-dependent flow for $v_2 \in \{0, 0.05, 0.10, 0.15, 0.20, 0.25\}$. This should be *one figure* with 6 curves. Use a time step of $\Delta t_1 = .01s$, and a final time of $T = 2.5s$. Remember that the material properties are a function of temperature!

PART 2: NOZZLE WEAR:

In order to simulate wear, you will calculate the radius at a function of time for 100 hours of continuous operation. For this part, we assume fully developed, laminar flow such that q is constant. We also steady state thermal conditions for the differential element in question. As such, the temperature will be a fixed constant $\theta(t) = \bar{\theta}$ for all time.

1. Show how to analytically solve for the steady state radius R_{ss} using equation 26, and assuming that $q = 2$. (*Hint: What is the rate of change of the nozzle radius at steady state?*)

2. Plot the normalized radius $\frac{R(t)}{R_o}$ as a function of time for $v_2 \in \{0, 0.05, 0.10, 0.15, 0.20, 0.25\}$. and $\bar{\theta} = 500\ K$. On the same figure, plot R_{ss}/R_o as a horizontal dashed line of the same color as its associated normalized radius curve. This should be *one figure* with 6 curves and 6 horizontal dashed lines. Please see example plot below for formatting. Use a time step of $\Delta t_2 = 3.6s$, and a final time of $T_2 = (100 \times 3600)s$. Remember that the material properties are now constant, since the temperature is now constant!

3. Plot the normalized radius $\frac{R(t)}{R_o}$ as a function of time for $\bar{\theta} \in \{300, 400, 500, 600, 700, 800\}\ K$. and $v_2 = 0.15$. On the same figure, plot R_{ss}/R_o as a horizontal dashed line of the same color as its associated normalized radius curve. This should be *one figure* with 6 curves and 6 horizontal dashed lines. Please see example plot below for formatting. Use a time step of $\Delta t_2 = 3.6s$, and a final time of $T_2 = (100 \times 3600)s$. Remember that the material properties now constant since the temperature is constant!

4. Plot the analytically determined R_{ss} as a function of the temperature for the range $\bar{\theta} \in \{300, 400, 500, 600, 700, 800\}\ K$ and for $v_2 \in \{0, 0.05, 0.10, 0.15, 0.20, 0.25\}$. This should be *one figure* with 6 curves. Based on this figure, does the volume fraction or the slurry temperature appear to have a larger effect on the nozzle wear? How are these results consistent with the theory developed in lecture?

5. Create a table comparing the percent difference[3] between $R(T)$ and R_{ss} for each combination of v_2 values and $\bar{\theta}$ values. In which cases is the difference smaller? What does a smaller difference physically represent?

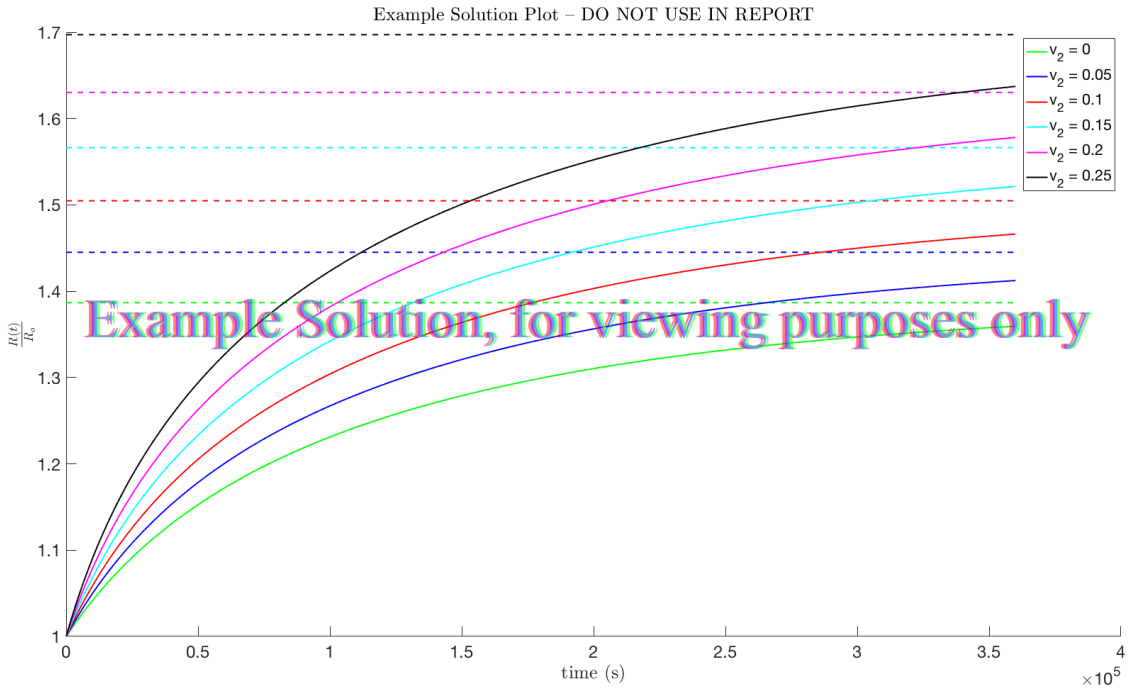

Figure 3.3: Example Solution Plot

[3] % difference $= 100 \times (R_{ss} - R(T))/R_{ss}$

PART 1 VARIABLE GLOSSARY

Symbol	Type	Units	Value	Description
$\mu_1 = \mu_{fo}$	Scalar	Pa s	.001	Phase 1 viscosity
σ_{fo}	Scalar	$\Omega^{-1}m^{-1}$	0.617	Reference temp. conductivity of fluid.
σ_{po}	Scalar	$\Omega^{-1}m^{-1}$	0.13	Reference temp. conductivity of particles.
$\rho_1 = \rho_{fo}$	Scalar	kg/m^3	2000	Phase 1 density
$\rho_2 = \rho_{po}$	Scalar	kg/m^3	4000	Phase 1 density
C_f	scalar	J/kg K	1600	Fluid heat capacity
C_p	scalar	J/kg K	3800	Particle heat capacity
c_1	Scalar	none	0.01	Flow profile parameter
c_2	Scalar	none	2	Flow profile parameter
R	Scalar	m	1e-3	Channel radius
Q_o	Scalar	m^3/s	1e-6	Base flow rate for part A
b	Scalar	none	.25	Flow rate parameter for part A
ω	Scalar	s^{-1}	12	Flow angular frequency.
h	scalar	W/(m^2 K)	10	Convective Heat transfer coefficient
θ_o	scalar	K	300	Initial Slurry Temperature
θ_a	scalar	K	300	Ambient Temperature
$\dot{\theta}$	scalar	K/s	50	Time Rate of change of temperature
Δt_1	scalar	s	0.01	Time Step Size
T	scalar	s	2.5	Total simulation time
a	scalar	none	0.8	absorption coefficient
$k_1,\ k_2,\ k_3$	scalar	unitless	0.5, 1, 2	Thermal softening parameters
v_2	scalar	none	$\{0, 0.05, 0.10, 0.15, 0.20, 0.25\}$	Particle Volume Fractions
ϕ	scalar	none	0.5	Hashin-Shtrikman Weight

PART 2 VARIABLE GLOSSARY

Symbol	Type	Units	Value	Description
$R(t=0)=R_0$	Scalar	m	0.001	Starting channel radius.
q	Scalar	unitless	2	Velocity Profile Coefficient
$v_m(t=0)$	Scalar	m / s	0.01	Initial mean velocity
Q_o	Scalar	m^3/s	$\int_{A_o} v\, dA = \pi R_o^2 v_m(t=0)$	Volumetric flow rate
μ_{fo}	Scalar	Pa s	0.001	Fluid viscosity
$\rho_1 = \rho_{fo}$	Scalar	kg/m^3	2000	Phase 1 density
$\rho_2 = \rho_{po}$	Scalar	kg/m^3	4000	Phase 1 density
$\bar{\theta}$	Scalar	K	See Instructions	Slurry Temperature
v_2	Scalar	unitless	See Instructions	Particle Volume Fraction
θ_o	Scalar	K	300	Initial Slurry Temperature
τ^{crit}	scalar	Pa	0.001	Wall detachment threshold stress
η	scalar	m/s	$10^{-5}/3600$	Wear rate constant
c_1	Scalar	none	0.01	Flow profile parameter
c_2	Scalar	none	2	Flow profile parameter
Δt_2	scalar	s	3.6	Time Step Size
T	scalar	s	3600×100	Time Step Size
$k_1,\ k_2,\ k_3$	scalar	unitless	0.5, 1, 2	Thermal softening parameters

4 Solution

The assignment solution is encoded in Matlab below.

```
close all
clear
clc
%% Assignment Part A: Pumping Pressure

%% Defining Constants

uf0 = 0.001; % Pudding viscosity (Pa-s)
sf0 = 5; % Salted Pudding Conductivity (S/m)
sp0 = 10^(-10); % Jelly Conductivity (S/m)
Qoo = 1E-6; % Nominal Volumetric flow rate (m^3/s)
rf = 1000; % Water density (kg/m^3)
rp = 6500;  % Particle density (kg/m^3)
R = 0.001; % Channel Radius (m)
c1 = 0.01; c2 = 2; % Profile Constants
a = 0.25; % Constant
b = 0.8; % Absorbtion Coefficient
T0 = 300; % Initial Temp (K)
omega = 12; % frequency (1/s)
v2 = 0:0.05: 0.25;% Volume fractions to loop over
t = linspace(0,2.5,1000); % Time to loop over (s)
dt = t(2)-t(1);
k1 = 0.5;
k2 = 1;
k3 = 2;
dx = 2*R;
V = 120/dx; % EMF (Volts/m)
phi = 0.5;
Cf = 4000; % Specific Heat of Fluid (J/kg-k)
Cp = 2000; % Specific Heat of Particles (J/kg-k)
h = 30; % Convection coef of air for forced convection (W/m^2-K)
Tenv = T0-100;
%% Looping through different volume fractions and times

% Initializing parameters to save for every v2 and time step
pGrad = zeros(numel(t),numel(v2)); % Pressure gradient
Re = zeros(numel(t),numel(v2)); % Reynolds number
q = zeros(numel(t),numel(v2)); % velocity profile exponent
T = T0*ones(numel(t),numel(v2));

for i = 1:numel(v2)
    % Calculate effective properties

    rstar = (1-v2(i))*rf + v2(i)*rp;
    Cstar = (1-v2(i))*Cf + v2(i)*Cp;



    % looping through the time steps
    for j = 1:(numel(t)-1)

```

```
52          Qo = Qoo*(1+a*sin(omega*t(j)));
53
54          uf = uf0*exp(-k1*((T(j)-T0)/T0));
55          s1 = sf0*exp(-k2*((T(j)-T0)/T0));
56          s2 = sp0*exp(-k3*((T(j)-T0)/T0));
57
58          s2sM = s1 + ((v2(i))./((1)./(s2-s1) + (((1-v2(i)))./(3*s1))));
59          s2sP = s2 + ((1-v2(i))./((1)./(s1-s2) + (((v2(i)))./(3*s2))));
60
61          ustar = uf*(1+2.5*(v2(i)/(1-v2(i))));
62          sstar = phi*s2sM + (1-phi)*s2sP;
63
64          J = V/sstar;
65
66          T(j+1,i) = T(j,i) + dt/(rstar*Cstar)*(b*(J^2)/sstar - h*(T(j,i)-Tenv))
                ;
67
68          % Effective Re scaled parameter
69          gstar = (2*c1*Qo*rstar)/(pi*R*ustar);
70
71          % Velocity profile constant
72          q(j+1,i) = 0.5*((gstar+c2) + sqrt((gstar+c2)^2 + 8*gstar));
73
74          % Maximum Centerline velocity (m/s)
75          vmax = (Qo*(q(j,i)+2))/(pi*q(j,i)*R^2);
76
77          Re(j+1,i) = (rstar*vmax*2*R)/(ustar);
78          pGrad(j+1,i) = ((2*ustar*(q(j,i)+2))/(pi*R^4))*Qo;
79      end
80  end
81
82
83  %% Plotting results
84
85  for i = 1:numel(v2)
86      % Plotting pressure gradient over time
87      figure(1)
88      plot(t,pGrad(:,i),'LineWidth',2)
89      hold on
90
91      % Plotting Re over time
92      figure(2)
93      plot(t,Re(:,i),'LineWidth',2)
94      hold on
95
96      % Plotting q
97      figure(5)
98      plot(t,q(:,i),'LineWidth',2)
99      hold on
100
101     figure(10)
102     plot(t,T(:,i),'LineWidth',2)
103     hold on
104 end
```

```
105
106 figure(1)
107 title('Time Evolution of Pressure Gradient','interpreter','Latex')
108 ylabel('$-\frac{\Delta p}{\Delta x}$ (Pa/m)','interpreter','Latex')
109 xlabel('time (s)','interpreter','Latex')
110 legend('v_2 = 0','v_2 = 0.05','v_2 = 0.10','v_2 = 0.15','v_2 = 0.20',...
111     'v_2 = 0.25')
112 set(gca,'FontSize',24)
113
114 figure(2)
115 title('Time Evolution of Reynolds Number','interpreter','Latex')
116 ylabel('$Re$','interpreter','Latex')
117 xlabel('time (s)','interpreter','Latex')
118 legend('v_2 = 0','v_2 = 0.05','v_2 = 0.10','v_2 = 0.15','v_2 = 0.20',...
119     'v_2 = 0.25')
120 set(gca,'FontSize',24)
121
122 figure(5)
123 title('Time Evolution of velocity profile exponent','interpreter','Latex')
124 ylabel('$q$','interpreter','Latex')
125 xlabel('time (s)','interpreter','Latex')
126 legend('v_2 = 0','v_2 = 0.05','v_2 = 0.10','v_2 = 0.15','v_2 = 0.20',...
127     'v_2 = 0.25')
128 set(gca,'FontSize',24)
129
130 figure(10)
131 title('Time Evolution of Temperature','interpreter','Latex')
132 ylabel('$\theta$','interpreter','Latex')
133 xlabel('time (s)','interpreter','Latex')
134 legend('v_2 = 0','v_2 = 0.05','v_2 = 0.10','v_2 = 0.15','v_2 = 0.20',...
135     'v_2 = 0.25')
136 set(gca,'FontSize',24)
137
138 %% Assignment Part B: Nozzle Wear
139
140 %% Defining Constants
141
142 Ro = 0.001; % Starting radius (m)
143 vmo = 0.01; % Initial Mean velocity (m/s)
144 Qo = pi*(Ro^2)*vmo; % Volumetric flow rate (m^3/s)
145 uf = 10.0; % Fluid Velocituy (Pa-s)
146 tcrit = 150; % Threshold Stress (Pa)
147 n = (10^-5)/(3600); % Wear Rate (m/s)
148 rf = 900; % Fluid Density (kg/m^3)
149 rp = 9000; % Particle Density (kg/m^3)
150 c1 = 0.01; c2 = 2; % Flow profile parameters
151 v2 = 0:0.05: 0.25;% Volume fractions to loop over
152 fac = 3600; % Time conversion factor (s/h)
153 dt = 0.001*fac; % Time step (s)
154 tf = 100*fac; % Final time (s)
155 t = 0:dt:tf; % Time to loop over (s)
156
157 %% Looping through different volume fractions and times
158
```

```
% Defining Rss symbolic
syms Rs

% Initializing parametes to save for every v2 and time step
Rss = zeros(numel(v2),1); % Steady state radius (m)
Rt = zeros(numel(t),numel(v2)); % Normalized Radius (m)
q = zeros(numel(t),numel(v2)); % velocity profile exponent
Rt(1,:) = Ro; % Initializing radius for all v2's


for i = 1:numel(v2)
    % Calculate effective properties
    ustar = uf*(1+2.5*(v2(i)/(1-v2(i))));
    rstar = (1-v2(i))*rf + v2(i)*rp;

    % Effective Re scaled parameter
    gstar = (2*c1*Qo*rstar)/(pi*Rs*ustar);

    % Velocity profile constant
    q1 = 0.5*((gstar+c2) + sqrt((gstar+c2)^2 + 8*gstar));

    % Calculate R steady state by approximation using intitial gstar and q
    % parameters
    Rss(i) = double(vpasolve(Rs == ((ustar*Qo*(q1+2))/(pi*tcrit))^(1/3),Rs));

    % looping through the time steps to update R(t)
    for j = 1:numel(t)-1
        % Effective Re scaled parameter
        gstar = (2*c1*Qo*rstar)/(pi*Rt(j,i)*ustar);

        % Velocity profile constant
        q(j,i) = 0.5*((gstar+c2) + sqrt((gstar+c2)^2 + 8*gstar));

        % Calculating Rdot
        Rdot = n*max([(((ustar*Qo*(q(j,i)+2))/(pi*tcrit*(Rt(j,i)^3))) - 1, 0]);
        Rt(j+1,i) = Rt(j,i) + dt*Rdot;
    end
end

% Calculating Error percentage
Rdiff = (abs(Rt(end,:) - Rss')./Rss')*100;

% growth term
Gt = Rt - Ro;

% normalizing over R0
Rt = Rt/Ro;
Gt = Gt / Ro;
Rss = Rss/Ro;


%% Plotting Results/Outputting error for table

% Colors for plotting
```

```
213 col1 = ['g' 'b' 'r' 'c' 'm' 'k'];
214 for i = 1:numel(v2)
215     % Plotting R(t)
216     figure(3)
217     hold on
218     h = plot(t,Rt(:,i),col1(i),...
219         'LineWidth',2,'DisplayName',['v_2 = ' num2str(v2(i))]);
220     hold on
221     plot(t,Rss(i)*ones(size(t))...
222         ,[col1(i) '--'],'LineWidth',2,'HandleVisibility','off');
223
224
225     % Plotting G(t)
226     figure(4)
227     plot(t,Gt(:,i),'LineWidth',2)
228     hold on
229 end
230
231
232 figure(3)
233 legend
234 title('Time Evolution of Normalized Nozzle Radius','interpreter','Latex')
235 ylabel('$\frac{R(t)}{R_o}$','interpreter','Latex')
236 xlabel('time (s)','interpreter','Latex')
237 % set(h,legend('v_2 = 0','v_2 = 0.05','v_2 = 0.10','v_2 = 0.15','v_2 =
        0.20',...
238 %     'v_2 = 0.25')
239 % legend('R(t) @ v_2 = 0',...
240 %     'R(t) @ v_2 = 0.05','R_{ss} @ v_2 = 0.05',...
241 %     'R(t) @ v_2 = 0.10','R_{ss} @ v_2 = 0.10',...
242 %     'R(t) @ v_2 = 0.15','R_{ss} @ v_2 = 0.15',...
243 %     'R(t) @ v_2 = 0.20','R_{ss} @ v_2 = 0.20', ...
244 %     'R(t) @ v_2 = 0.25','R_{ss} @ v_2 = 0.25')
245 set(gca,'FontSize',24)
246
247 figure(4)
248 title('Time Evolution of Normalized Nozzle Growth','interpreter','Latex')
249 ylabel('$\frac{G(t)}{R_o}$','interpreter','Latex')
250 xlabel('time (s)','interpreter','Latex')
251 legend('v_2 = 0','v_2 = 0.05','v_2 = 0.10','v_2 = 0.15','v_2 = 0.20',...
252     'v_2 = 0.25')
253 set(gca,'FontSize',24)
254
255 disp('Error With v2 value in top row and error value (m) in bottom row')
256 display([v2; Rdiff])
```

5 Ethical Considerations for this Project

A goal of this project is to enable advancements in science and engineering through to address critical national challenges associated with next generation food systems. There are deep ethical considerations associated with any technology, in particular for food systems. While technology has tremendous potential to identify greater efficiencies, when it is created without appropriate consideration for who will have access to and control over new resources, or how the new technologies will impact those who work in the system, the efficiencies identified may come at the cost of greater societal inequity. It is important to pursue harnessing technology to disrupt existing inequities, rather than further entrench existing power structures. The following areas should be considered:

- Labor: 1) occupational health, 2) food manufacturing, and 3) outdoor agriculture labor;
- Producers: 1) Small- to mid-size farms, 2) urban agriculture, and 3) research in farm transitions; Technology: 1) research in technology and democracy;
- Health Human Rights: 1) land rights, 2) social justice, and 3) decolonization in agriculture;

Please consider the following questions:

- What are the societal implications of the technology that you are developing?
- Can this technology be distributed fairly and equitably to a wide variety of entities in agricultural industry?
- Are there any potential unintended consequences of this technology becoming available?
- Are there any harmful "spinoffs" of this technology?
- Are there any useful "spinoffs" of this technology?

6 References

1. Avci, B. & Wriggers, P. 2012 A DEM-FEM coupling approach for the direct numerical simulation of 3D particulate flows, Journal of Applied Mechanics, Vol. 79, 010901-(1-7).

2. Ahmad, Z., Rasekh, M., Edirisinghe, M. 2010 Electrohydrodynamic Direct Writing of Biomedical Polymers & Composites. Macromolecular Materials & Engineering. 295, 315-319.

3. Choi, S., Park, I., Hao, Z., Holman, H. Y., Pisano, A. P. & Zohdi, T. I. 2010 Ultra-fast self-assembly of micro-scale particles by open channel flow. *Langmuir.* 26 (7), pp 4661-4667.

4. Choi, S., Stassi, S., Pisano, A. P. & Zohdi, T. I. 2010 Coffee-Ring Effect-Based Three Dimensional Patterning of Micro, Nanoparticle Assembly with a Single Droplet. *Langmuir.* 26 (14), pp 11690-11698.

5. Choi, S., Jamshidi, A., Seok, T. J., Zohdi, T. I., Wu., M. C., & Pisano, A. P. 2012 Fast, High-throughput creation of size-tunable micro, nanoparticle clusters via evaporative self-assembly in picoliter-scale droplets of particle suspension. Langmuir. 28(6):3102-11.

6. Choi, S., Pisano, A. P. & Zohdi. T. I. 2013 An Analysis of Evaporative Self-Assembly of Micro Particles in Printed Picoliter Suspension Droplets. Journal of Thin Solid Films. Volume 537, 30, Pages 180-189.

7. Demko, M. T., Cheng, J. C., & Pisano, A. P. 2010 High-Resolution Direct Patterning of Gold Nanoparticles by the Microfluidic Molding Process. Langmuir, pp. 412-417.

8. Demko, M. T., Choi, S. Zohdi, T. I. & Pisano, A. P. 2012 High resolution patterning of nanoparticles by evaporative self-assembly enabled by in-situ creation & mechanical lift-off of a polymer template. *Applied Physics Letters.* 99, 253102-1-253102-3.

9. Einstein, A. 1906 A new determination of molecular dimensions. Annals of Physics, 19(4), 289–306.

10. Fuller, S. B., Wilhelm, E. J.; Jacobson, J. M. 2002 Ink-jet printed nanoparticle microelectromechanical systems. Journal of Microelectromechanical Systems, 11, 54-60.

11. Hashin, Z. & Shtrikman, S. 1962 On some variational principles in anisotropic & nonhomogeneous elasticity. Journal of the Mechanics & Physics of Solids. **10**, 335-342.

12. Hashin, Z. & Shtrikman, S. 1963 A variational approach to the theory of the elastic behaviour of multiphase materials. Journal of the Mechanics & Physics of Solids. **11**, 127-140.

13. Hashin, Z. 1983 Analysis of composite materials: a survey. ASME Journal of Applied Mechanics. **50**, 481-505.

14. Hinze, J. O. 1975 Turbulence. McGraw-Hill. New York.

15. Kachanov, M. & Abedian, B. 2015 On the isotropic & anisotropic viscosity of suspensions containing particles of diverse shapes & orientations. *International Journal of Engineering Science*, Volume 94, Pages 71-85.

16. Leonardi, A., Wittel, F. K., Mendoza, M & Herrmann, H. J. 2014 Coupled DEM-LBM method for the free-surface simulation of heterogeneous suspensions. Computational Particle Mechanics, Volume 1, Issue 1, pp 3-13.

17. Martin, P. 2009 Handbook of deposition technologies for films & coatings. 3rd Ed. Elsevier.

18. Martin, P. 2011 Introduction to surface engineering & functionally engineered materials. Scrivener & Elsevier.

19. Onate, E., Celigueta, M. A., Latorre, S., Casas, G., Rossi, R. & Rojek, J. 2014 Lagrangian analysis of multiscale particulate flows with the particle finite element method Computational Particle Mechanics, Volume 1, Issue 1, pp 85-102.

20. Park, J. U., Hardy, M., Kang, S. J., Barton, K., Adair, K., Mukhopadhyay, D. K., Lee, C. Y., Strano, M. S., Alleyne, A. G., Georgiadis, J. G., Ferreira, P. M. & Rogers, J. A. 2007 High-resolution electrohydrodynamic jet printing. Nature Materials. 6, 782-789.

21. Park, I., Ko, S. H., Pan, H., Grigoropoulos, C. P., Pisano, A. P., Frechet, J. M. J., Lee, E. S. & Jeong, J. H. 2008 Nanoscale Patterning & Electronics on Flexible Substrate by Direct Nanoimprinting of Metallic Nanoparticles. Advanced Materials. 20, 489.

22. Probstein, R. (2003). Physiochemical hydrodynamics: an introduction. 2nd Edition. Wiley.

23. Samarasinghe, S. R., Pastoriza-Santos, I., Edirisinghe, M. J., Reece, M. J., Liz-Marzan, L. M. 2006 Printing Gold Nanoparticles with an Electrohydrodynamic Direct Write Device. Gold Bulletin. 39, 48-53.

24. Sevostianov, I. & Kachanov, M. 2012 Effective properties of heterogeneous materials: Proper application of the non-interaction & the "dilute limit" approximations. *The International Journal of Engineering Science.* Volume 58, 124-128.

25. Torquato, S. 2002 Random Heterogeneous Materials: Microstructure & Macroscopic Properties Springer-Verlag, New York.

26. Zohdi, T. I. & Wriggers, P. 2008 Introduction to computational micromechanics. Springer-Verlag.

27. Zohdi, T. I. 2014 Embedded electromagnetically sensitive particle motion in functionalized fluids. *Computational Particle Mechanics.* Vol 1, 27-45.